

### Numerical Heat Transfer, Part A: Applications



ISSN: 1040-7782 (Print) 1521-0634 (Online) Journal homepage: http://www.tandfonline.com/loi/unht20

# TURBULENT CONVECTION HEAT TRANSFER IN LONGITUDINALLY CONDUCTING, EXTERNALLY FINNED PIPES

F. Moukalled, J. Kasamani & S. Acharya

To cite this article: F. Moukalled, J. Kasamani & S. Acharya (1992) TURBULENT CONVECTION HEAT TRANSFER IN LONGITUDINALLY CONDUCTING, EXTERNALLY FINNED PIPES, Numerical Heat Transfer, Part A: Applications, 21:4, 401-421, DOI: 10.1080/10407789208944884

To link to this article: http://dx.doi.org/10.1080/10407789208944884

	Published online: 30 Mar 2007.
	Submit your article to this journal 🗗
ılıl	Article views: 14
a a	View related articles 🗹
4	Citing articles: 7 View citing articles 🗷

Full Terms & Conditions of access and use can be found at http://www.tandfonline.com/action/journalInformation?journalCode=unht20

## TURBULENT CONVECTION HEAT TRANSFER IN LONGITUDINALLY CONDUCTING, EXTERNALLY FINNED PIPES

#### F. Moukalled and J. Kasamani

Mechanical Engineering Department, American University of Beirut, Beirut, Lebanon

#### S. Acharya

Mechanical Engineering Department, Louisiana State University, Baton Rouge, Louisiana 70803

A numerical investigation is conducted of turbulent convection in a longitudinally conducting, externally finned pipe. Results reveal significant enhancement in heat transfer due to finning. The heat transfer rate to the fluid increases with increasing thermal conductivity of the pipe wall, with increasing values of the external heat transfer coefficient, and with decreasing interfin spacing. Heat transfer is underestimated by as much as 30 times in the developed region when the thermal conductivity of the pipe wall is not accounted for. The magnitude of this underestimation decreases with decreasing wall conductivity. Finning is found to be most effective at low values of wall conductivity, where a nearly 10-fold increase in heat transfer is noted. At high thermal conductivities in the wall, the Nusselt number and the pipe wall temperature vary monotonically in the axial direction, and this variation becomes increasingly nonmonotonic at lower thermal conductivities. A constant, spatially averaged, Biot number solution is found to give satisfactory results only for cases of high conductivity in the wall. The asymptotically developed Nusselt numbers compare well (within 7%) with the axially averaged values for the cases of conducting pipe wall.

#### INTRODUCTION

The objective of this study is to predict the heat transfer characteristics of turbulent fluid flow in longitudinally conducting, externally finned pipes. Flows through externally finned pipes are encountered in many heat exchange applications. The fins are generally square plates or annular plates distributed uniformly on the outer surface of the pipe and enhance heat transfer by increasing the heat transfer surface area. Consequently, the outer surface of the finned pipe can be idealized as a surface with a spatially periodic boundary condition, a low heat transfer coefficient  $(h_t)$  along the unfinned sections, and a high heat transfer coefficient  $(h_t)$  along the finned sections. Figure 1a shows a schematic of the finned pipe, and Fig. 1b shows the above-described model for the variation of the heat transfer coefficient.

Laminar heat transfer in externally finned pipes has been studied recently. Sparrow

This work was initiated in the Mechanical Engineering Department at Louisiana State University and completed in the Mechanical Engineering Department at the American University of Beirut. It was partially supported by the University Research Board of the American University of Beirut under grant 18-4209.

```
NOMENCLATURE
 Bi
                       Biot number (-hR_o/k)
                                                                                                                                                                                                                      parameter appearing in Eq. (11) \{ = \alpha | Bi = \alpha
                                                                                                                                                                                                                      \beta(\partial\theta/\partial\eta)_{n-1}
h
                       heat transfer coefficient
k
                                                                                                                                                                                                                      dimensionless radial coordinate (=r/R_i)
                       thermal conductivity
                       mixing length
                                                                                                                                                                                                                      dimensionless temperature [-(T - T_{in})/
Nu
                      local Nusselt number
                                                                                                                                                                                                                     (T_{\infty} - T_{\rm in})
                       pressure
                                                                                                                                                                                                                      viscosity
 P
                       dimensionless pressure (-p/\rho \bar{u}^2)
                                                                                                                                                                                                                     density
 Pe
                      Péclet number
                                                                                                                                                                                                                     dimensionless interfin spacing (-s/R_i
 Pr
                       Prandtl number
                      rate of heat transfer between x = 0 and
 Q
                                                                                                                                                                                                                     dimensionless fin thickness (=t/R_i Pe)
                      x - x
                                                                                                                                                                                                                      wall shear stress
                       radial coordinate
 R_{i}
                      inner radius of pipe
                                                                                                                                                                                               Subscripts
R_{\rm o}
                       outer radius of pipe
Re.
                       Reynolds number (-\rho u_m R_i/\mu)
                       interfin spacing
s
                                                                                                                                                                                                                     average value
                                                                                                                                                                                              a
                       fin thickness
                                                                                                                                                                                                                     finned section
T
                       temperature
                                                                                                                                                                                               fd
                                                                                                                                                                                                                     fully developed
и
                      time-averaged component of axial velocity
                                                                                                                                                                                              fl
                                                                                                                                                                                                                     fluid property
                      mean value of u at any axial location
                                                                                                                                                                                                                     condition at inner radius
u_{\rm m}
                                                                                                                                                                                              i
U
                      dimensionless axial velocity (=u/u_m)
                                                                                                                                                                                                                     condition at inlet
                                                                                                                                                                                              in
                      axial coordinate
                                                                                                                                                                                                                     laminar flow
x
X
                      dimensionless axial coordinate [-x/(R_i Pe)]
                                                                                                                                                                                                                     maximum value
                                                                                                                                                                                               max
                      distance from pipe wall
                                                                                                                                                                                               0
                                                                                                                                                                                                                     condition at outer radius
                       parameter appearing in Eq. (11) \{-2 \text{ Pe}^2/
                                                                                                                                                                                                                     turbulent flow
α
                                                                                                                                                                                              ŧ
                       [(R_{\rm o}/R_{\rm i})^2 - 1]
                                                                                                                                                                                                                     unfinned section
                                                                                                                                                                                               u
β
                       fluid to wall thermal conductivity ratio
                                                                                                                                                                                               w
                                                                                                                                                                                                                     wall property
                       (-k_{\rm fl}/k_{\rm w})
                                                                                                                                                                                                                     ambient condition
                                                                                                                                                                                               00
```

and Charmchi [1] investigated the behavior of laminar heat transfer in externally finned pipes but neglected the effect of axial conduction in the pipe wall. No calculations for turbulent flows were performed in their study. Moukalled and Acharya [2] extended the work reported by Sparrow and Charmchi [1] by including the effect of conduction in the pipe wall. The significant influence of axial wall conduction on the heat transfer behavior was clearly demonstrated. However, the results reported by Moukalled and Acharya [2] are again limited to laminar, hydrodynamically fully developed flow.

A few studies have also been reported on flow and heat transfer through longitudinally conducting, smooth, unfinned pipes. Lin and Chow [3] obtained an analytical solution for turbulent flow and heat transfer in an unfinned pipe, taking into account the effects of axial and radial conduction in the pipe wall. Faghri and Sparrow [4] considered simultaneous wall and fluid axial conduction in laminar pipe flow and heat transfer. Depending on the wall conductance parameter and the Péclet number, it was found that axial wall conduction can carry a substantial amount of heat upstream into the non-directly heated portion of the pipe. Anand and Tree [5] have numerically studied the effect of axial conduction in a tube wall with a step change in heat flux. Fithen and Anand [6] used a finite-element technique to study conjugate pipe flow and heat transfer. Barozzi and Pagliarini [7] used a superposition principle with a finite-element method to

solve conjugate heat transfer in a pipe. Soliman [8] presented an analytical solution for slug flow with wall conduction, while Zariffeh et al. [9] used a numerical method to solve for flow in a tube with axial wall and fluid conduction.

In this paper, as noted before, axial conduction in the wall of an externally finned pipe is accounted for, and its influence on turbulent convection heat transfer is assessed. Since in most practical situations the flow is turbulent, the earlier laminar flow study of Moukalled and Acharya [2] has limited applicability, and this paper addresses the more commonly encountered situation of turbulent flow in an externally finned pipe. Radial conduction in the pipe wall is neglected, and therefore results are valid for relatively thin pipes. In view of the axial conduction, a conjugate heat transfer problem has to be solved. In this work, this solution is obtained by a numerical technique. The coupling between turbulent convection in the pipe and conduction in the pipe wall is accomplished by ensuring continuity of the thermal conditions along the inside surface of the pipe. These conditions are not known beforehand and have to be determined along with the solution to the problem. This adds to the complexity of the problem and necessitates the use of an iterative procedure in which the fluid convection and the pipe conduction equations are successively solved until convergence. To model turbulence, the mixing length theory is used. As discussed later, for simple pipe flows such a model is adequate.

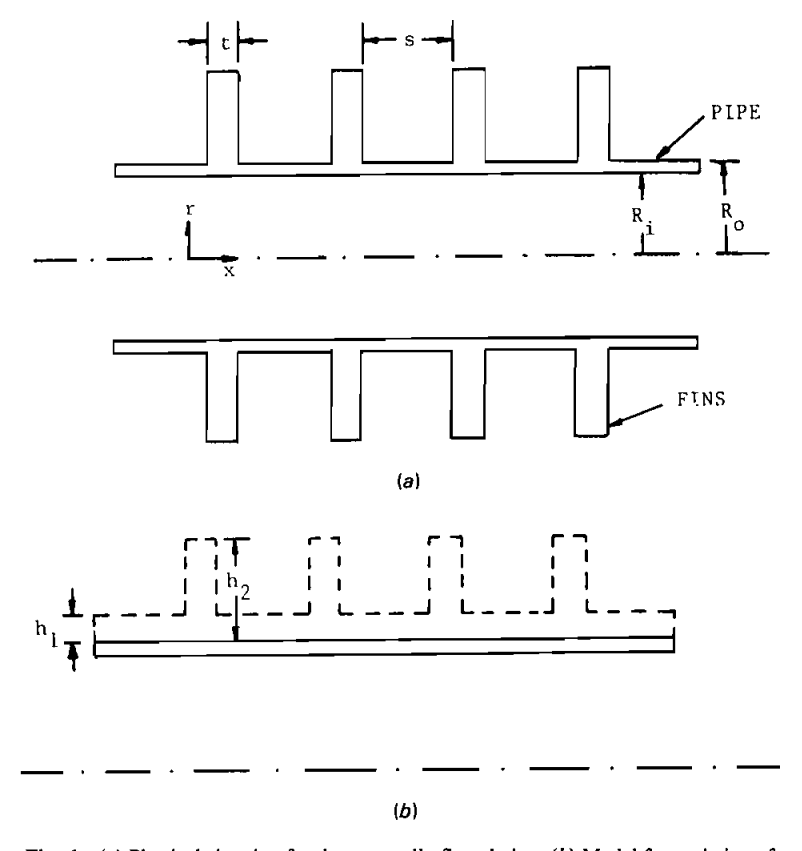


Fig. 1 (a) Physical situation for the externally finned pipe. (b) Model for variation of the heat transfer coefficient.

Due to the lack of any numerical or experimental data for the specific problem considered herein, comparison is made with predictions obtained for an unfinned tube and with those calculated for the spatially averaged values of the high and low external Biot numbers.

#### **GOVERNING EQUATIONS**

The physical situation under consideration is illustrated in Fig. 1a (and is modeled as shown in Fig. 1b) and represents turbulent convection of a fluid in a longitudinally conducting, externally finned pipe. Fluid enters the pipe with an assumed uniform temperature  $T_{\rm in}$  that is different from the ambient temperature  $T_{\infty}$ . The governing equations for conservation of momentum and energy are formulated for hydrodynamically fully developed turbulent flow. Water is assumed to be the working fluid, and all property values are chosen to correspond to water.

Instead of using an analytical or experimental velocity profile for the hydrodynamically fully developed turbulent flow, a numerical solution is first obtained of the momentum equation, using a uniform velocity profile at the inlet to the pipe and marching downstream until a fully developed turbulent velocity profile is obtained. Then this velocity profile is used to solve the energy equation. Moreover, axial diffusion in the fluid is neglected due to the high values of Péclet numbers in turbulent flow ( $\gg 50$ ). With these assumptions, the conservation of the x momentum equation and the conservation of energy equations can be expressed in parabolic form.

#### **Velocity Equation**

As noted above, the equation for conservation of the x momentum is solved first, until a fully developed velocity profile is obtained. This profile is then used in the conservation of energy equation. To express the governing equations in dimensionless form, the following dimensionless quantities are defined:

$$X = \frac{x}{R_i \text{ Pe}}$$
  $\eta = \frac{r}{R_i}$   $U = \frac{u}{u_m}$   $P = \frac{p}{\rho u_m^2}$  (1)

With these dimensionless variables, conservation of the x momentum equation becomes

$$\bar{\mathbf{U}} \cdot \nabla U = -\frac{\partial P}{\partial X} + \left(\frac{1}{\eta}\right) \frac{\partial}{\partial \eta} \left[ \Pr_{i} \left(1 + \frac{\mu_{i}}{\mu_{i}}\right) \frac{\eta}{\partial \eta} \frac{\partial U}{\partial \eta} \right]$$
 (2)

where  $\mu_1$  and  $\mu_1$  are the molecular and turbulent viscosities, respectively. For turbulent pipe flows, Re =  $5.5 \times 10^4$  is a typical value and is used here.

To solve the above conservation equation, which has a parabolic form, the boundary conditions and the turbulent viscosity  $\mu_t$  must be specified. The boundary conditions are

$$U = 1 \qquad \text{at } X = 0 \tag{3a}$$

$$\frac{\partial U}{\partial X} = 0 \quad \text{at } \eta = 0 \tag{3b}$$

$$U = 0 \qquad \text{at } \eta = 1 \tag{3c}$$

#### **Turbulence Model**

The turbulence model employed here is Prandtl's mixing length model [10, 11]. For simple pipe flows, such as those considered in this study, this model has been shown to be adequate. It is emphasized that while the choice of this model is based partly on its simplicity for pipe flows, the model is clearly adequate to determine the mean velocity profile of the flow. In a more complex flow situation, the use of the mixing length model could not have been justified. In this model, the turbulent viscosity  $\mu_t$  is evaluated in terms of the mixing length and the local velocity gradient. A commonly used representation for  $\mu_t$  is

$$\mu_{\rm t} = \rho \iota^2 \left| \frac{du}{dy} \right| \tag{4}$$

where  $\iota$  is the mixing length at a point situated at a distance y from the pipe wall and is represented as the product of a Nikuradse-type mixing length  $l_n$  [12] and a Van Driest [13] damping factor  $d_i$ , that is,

$$\iota = l_n d_f \tag{5}$$

For turbulent pipe flow,  $l_n$  and  $d_f$  are given by [10]

$$\frac{I_{\rm n}}{R_{\rm i}} = 0.14 - 0.08 \left(1 - \frac{y}{R_{\rm i}}\right)^2 - 0.06 \left(1 - \frac{y}{R_{\rm i}}\right)^4 \tag{6}$$

$$d_{\rm f} = 1 - \exp\left[-\left(\frac{\rho y}{26\mu_{\rm I}}\right)\left(\frac{\tau_{\rm w}}{\rho}\right)^{1/2}\right] \tag{7}$$

In the above equation,  $\tau_w$  is the local shear stress on the pipe wall. When Eqs. (5)-(7) are combined, the mixing length  $\iota$  and, consequently,  $\mu_{\iota}$  [Eq. (4)] are completely specified.

#### **Temperature Equation**

The conservation of energy equation in the fluid, in nondimensional form, can be written as

$$U\frac{\partial\theta}{\partial x} = \left(\frac{1}{\eta}\right)\frac{\partial}{\partial\eta}\left[\left(1 + \frac{\mu_t}{\mu_1}\frac{\mathrm{Pr}_1}{\mathrm{Pr}_1}\right)\frac{\eta}{\partial\eta}\frac{\partial\theta}{\partial\eta}\right] \tag{8}$$

where the nondimensional temperature  $\theta$  is defined as

$$\theta = \frac{T - T_{\rm in}}{T_{\infty} - T_{\rm in}} \tag{9}$$

and Pr<sub>1</sub> is the laminar Prandtl number and Pr<sub>1</sub> is the turbulent Prandtl number. Values representative for water have been assigned. The boundary conditions for the temperature equation are

$$\theta = 0 \qquad \text{at } X = 0 \tag{10a}$$

$$\frac{\partial \theta}{\partial \eta} = 0 \qquad \text{at } \eta = 0 \tag{10b}$$

$$\theta = \theta_{w}(X) \quad \text{at } \eta = 1 \tag{10c}$$

where  $\theta_w(X)$  is the temperature distribution in the pipe wall, which is not known a priori but is determined as part of the solution by solving the pipe wall conduction equation.

#### **Wall Conduction Equation**

The heat conduction equation for the pipe wall is formulated by making a quasione-dimensional energy balance on a control volume along the wall of the pipe. Pipe walls are assumed to be thin, so that radial temperature variations in the pipe wall can be assumed to be small. The final form of this equation can be expressed as

$$\frac{\partial^2 \theta_{w}}{\partial X^2} - \alpha \operatorname{Bi} \theta_{w} + \gamma = 0 \tag{11}$$

where

$$\alpha = \frac{2 \operatorname{Pe}^2}{(R/R)^2 - 1} \tag{12a}$$

$$\beta = \frac{k_{\rm fl}}{k_{\rm w}} \tag{12b}$$

$$\gamma = \alpha \left[ \text{Bi } - \beta \left( \frac{\partial \theta}{\partial \eta} \right)_{\eta - 1} \right]$$
 (12c)

and Bi is the Biot number, which varies periodically on the outside surface of the pipe and is equal to Bi, for the unfinned surface and Bi, for the finned surface. That is,

Bi = Bi<sub>u</sub> = 
$$\frac{h_u R_o}{k_w}$$
  $n(\sigma + \tau) < X < n(\sigma + \tau) + \sigma$  (13a)

Bi = Bi<sub>f</sub> = 
$$\frac{h_f R_o}{k_w}$$
  $n(\sigma + \tau) + \sigma < X < (n + 1)(\sigma + \tau) + \sigma$  (13b)

where

$$\sigma = \frac{s}{R_i \text{ Pe}}$$
  $\tau = \frac{t}{R_i \text{ Pe}}$   $n = 0, 1, 2, 3, \dots,$  (14)

The terms s and t are the interfin spacing and the fin thickness, respectively.

The thermal wall boundary conditions at the two ends of the pipe, X = 0 and  $X = L_p$ , also have to be specified. Due to lack of better information, it is assumed here that poorly conducting pipes (e.g., a CPVC pipe) are connected upstream and downstream of the externally finned pipe section. Such boundary conditions have also been used by many other workers [2-4]. Mathematically, the boundary condition can be written

$$\frac{\partial \theta_{w}}{\partial X} = 0 \quad \text{at } X = 0 \text{ and } X = L_{p}$$
 (15)

Another reasonable boundary condition at X=0 is to assume that the fluid and pipe wall are isothermal to  $T_0$ . This is equivalent to  $\theta_w=0$  at X=0. Since at X=0, the velocity profile has been taken to be fully developed, it has been implicitly assumed that the pipe upstream of X=0 is long enough for the flow to become fully developed, and the pipe and the fluid can therefore be assumed to be in thermal equilibrium, that is,  $\theta_w=0$  at X=0. Computations using this boundary condition have also been obtained, but for two cases only, and are used for the purpose of comparing results with those obtained using the previous boundary condition  $(\partial \theta_w/\partial X=0)$ .

It should be noted that the term  $(\partial \theta/\partial \eta)_{\eta=1}$  appearing in Eq. (12c) provides the coupling between the fluid and the pipe wall temperatures. This term is not known beforehand and is determined in the course of the solution.

Examination of the dimensionless governing equations and boundary conditions reveals the presence of six parameters, namely, the thermal conductivity ratio  $\beta$ , the low and high Biot numbers (Bi<sub>u</sub> and Bi<sub>f</sub>, respectively), the interfin spacing  $\sigma$ , the fin thickness  $\tau$ , the pipe radius ratio  $R_i/R_o$ , and the dimensionless pipe length  $L_p$ . To reduce the number of parameters,  $R_i/R_o$  is assigned the value of 0.9 (for thin pipes) and  $L_p$  (=  $l_p/R_i$  Pe) is assigned the value of 0.0015 (which is the length required for thermally fully developed flow when axial conduction is neglected). Other parameter values are listed in Table 1.

#### SOLUTION PROCEDURE AND COMPUTATIONAL DETAILS

The fluid momentum and energy equations, Eqs. (2) and (8), are solved numerically by the parabolic calculation procedure of Patankar and Spalding [14]. This is a fully implicit, marching-type solution procedure, proceeding from the inlet location (X = 0) to the exit of the pipe  $(X = L_p)$ . The equation for heat conduction in the pipe wall, Eq. (11), is solved by the elliptic finite-volume method described by Patankar [15].

The momentum equation, Eq. (2), is first solved separately to obtain the fully developed, turbulent velocity profile used in the fluid energy equation. Then an iterative approach is adopted, whereby the energy equation for the fluid and that for the pipe wall are solved consecutively. To start the first iteration, the fluid energy equation, Eq. (8), is

Table 1 Parameter Values

Case	$\beta \times 10^3$	τ	σ	Bi <sub>u</sub>	$\mathrm{Bi}_{\mathrm{f}}$	Case	Bi <sub>a</sub> [Eq. (16)]
1	00	$7.5 \times 10^{-7}$	3τ	1	50	 1A	53/4
2	16.5	$7.5 \times 10^{-7}$	$3\tau$	1	50	2A	53/4
3	1.65	$7.5 \times 10^{-7}$	$3\tau$	1	50	3A	53/4
4	<b>∞</b>	$7.5 \times 10^{-7}$	3τ	5	250	4A	265/4
5	16.5	$7.5 \times 10^{-7}$	$3\tau$	5	250	5A	265/4
6	1.65	$7.5 \times 10^{-7}$	$3\tau$	5	250	6A	265/4
7	<b>∞</b>	$7.5 \times 10^{-7}$	$7\tau$	1	50	7A	57/8
8	16.5	$7.5 \times 10^{-7}$	$7\tau$	1	50	8A	57/8
9	1.65	$7.5 \times 10^{-7}$	$7\tau$	1	50	9A	57/8

solved by imposing a guessed value for  $\theta_w(X)$  as the boundary condition needed in Eq. (10c). The solution obtained is fed into the pipe wall conduction equation, Eq. (11), via the term  $(\partial \theta/\partial \eta)_{\eta=1}$ , which is solved to obtain updated values for  $\theta_w(X)$ . The updated  $\theta_w(X)$  is used to initiate the second iteration, and the fluid energy equation is solved again. This procedure is continued until convergence to at least four significant figures is reached.

The computational task is fairly demanding in terms of both computer time and computer storage. This is mainly due to the periodic boundary condition, Eqs. (13a) and (13b), and the consecutive iterative scheme used to resolve conduction-convection coupling. The thermal boundary layer that develops each time a finned segment is encountered necessitates the use of a very small forward step size, especially in the initial portion of the pipe, where the largest differences occur between the fluid bulk temperature  $T_{\rm b}$  and the ambient temperature  $T_{\infty}$ . The flow computations are performed with 100 grid points, which span the pipe cross section  $0 \le \eta \le 1$ , and cluster more densely near the pipe wall. Nonuniform step sizes are used in the axial direction, and the value gradually increases in the streamwise direction. For the first 1000 steps, the forward step size was taken to be  $10^{-6}$ , then increased in steps up to  $8 \times 10^{-6}$ , and held constant thereafter. A total of 6100 points in the streamwise direction are used and, as discussed below, the 6100 × 100 mesh used is found to be adequate for producing gridindependent results. For the solution of the pipe wall conduction equation, 6100 grid points are used also. The conduction control volume faces were chosen to be identical to the streamwise positions in the flow solution. Thus the information transfer between the conduction and flow solutions can be easily done without the need for interpolation.

To check the accuracy of the solution, results were first calculated for the laminar case and compared with those reported by Sparrow and Charmchi [1] and Moukalled and Acharya [2]. Excellent agreement to within 0.75% was obtained. Also, the turbulent flow problem in an isothermal pipe was solved with the mixing length model, and results (Fig. 2) were found to be in excellent agreement with the experimental data of Nikuradse [12]. As a further check for accuracy, computations were performed using much smaller forward step sizes, a starting forward step value of  $10^{-12}$ , 200 grid points in the radial direction, and 12,200 grid points in the conduction problem. Results on the finer mesh (Fig. 2) agreed to within 0.8% of the results reported here.

#### **RESULTS AND DISCUSSION**

Due to the large number of parameters involved and lengthy computations needed for each set of parameters, a limited set of illustrative cases is considered.

As previously stated, the momentum equation is solved first to obtain the numerical turbulent fully developed velocity profile, which is used in all subsequent computations of the energy equation. As shown in Fig. 2, the computed velocity profile compares well with the measured velocity profile of Nikuradse [12].

Three values for the thermal conductivity ratio  $\beta$  are considered: the first case  $(\beta = \infty)$  represents the situation when axial conduction in the pipe wall is neglected, the second case  $(\beta = 16.5 \times 10^{-3})$  corresponds to a low wall conductivity situation,  $k_w = 40 \text{ W/m}$  °C (conductivity for steel), and the last case  $(\beta = 1.65 \times 10^{-3})$  characterizes a high wall conductivity situation,  $k_w = 400 \text{ W/m}$  °C (conductivity for copper). For all cases, the fluid thermal conductivity  $k_{\rm fl}$  is taken to be 0.66 W/m °C, corresponding to water. The choices for  $\tau$ ,  $\sigma$ , Bi<sub>u</sub>, and Bi<sub>t</sub> are essentially the same as those made by Moukalled and Acharya [2]. A listing of the various cases studied is presented in Table 1.

In the following discusison, cases 1, 4, and 7 represent the situations when axial conduction is neglected; cases 2, 5, and 8 are for pipes with wall thermal conductivity; and cases 3, 6, and 9 are for pipes with high wall thermal conductivity. Cases 1, 2, and 3 represent an interfin spacing that is 3 times the fin thickness and an external heat transfer coefficient along the finned section that is 50 times that of the unfinned part of the pipe. These are the baseline cases against which other cases are compared. Cases 4, 5, and 6 explore the effect on heat transfer of increasing the level of heat transfer coefficients  $h_0$ 

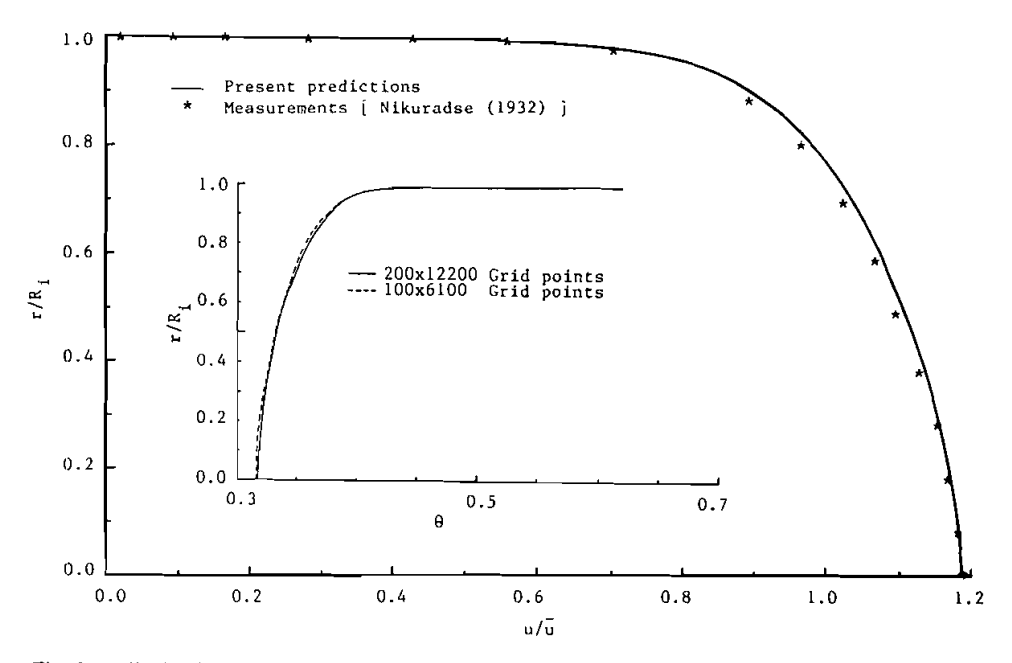


Fig. 2 Fully developed turbulent velocity profile based on mixing length theory (main figure) and temperature profile  $(X = 1.43 \times 10^{-3}, \text{case 2})$  for two different mesh spacings and forward step sizes (inset).

and  $h_f$ , keeping the same values for  $\tau$ ,  $\sigma$ , and the ratio  $h_f/h_u$ . Cases 7, 8, and 9 delineate the effect of increasing the interfin spacing to 7 times the fin thickness as compared with 3 times the fin thickness for cases 1, 2, and 3. For completeness, constant Biot number computations are included that correspond to the spatial average of  $Bi_u$  and  $Bi_f$  given by

$$Bi_{a} = \frac{\sigma Bi_{u} + \tau Bi_{f}}{\sigma + \tau}$$
 (16)

Results are intended to show heat transfer enhancement due to finning and to reveal the relative effects of axial conduction in the pipe wall and of the various parameters involved. For this purpose, calculations are performed to determine the bulk temperature and Nusselt number variations. Also included are the cross-stream fluid temperature profiles and the pipe wall temperature distribution.

#### **Bulk Temperatures**

The streamwise variation of the fluid bulk temperature, which also represents the fraction of the maximum possible heat that can be transferred to the fluid, can be written as

$$\theta_{\rm bx} = \frac{Q}{Q_{\rm max}} = 2 \int_0^1 U \theta \eta \ d\eta \tag{17}$$

As mentioned earlier, two boundary conditions at X = 0 are considered for the solution of the conduction equation, Eq. (11). The primary boundary condition used in obtaining the results is the adiabatic condition  $\partial \theta_w / \partial X = 0$ . Limited calculations are done with the isothermal boundary condition  $\theta_w = 0$ . The comparison between the two boundary conditions is depicted in Fig. 3. It may be noted that the curves for the adiabatic boundary condition are slightly higher than those for the isothermal boundary condition, but only near the entrance to the pipe, and after the initial entry region, the two curves merge into one. This result is expected, since the finned pipe section is insulated at the inlet and the pipe wall temperature there will be higher. Higher fluid bulk temperatures thus occur near the inlet for the adiabatic boundary condition case in comparison with the isothermal boundary condition situation. This difference is reduced in the streamwise direction with the increase in pipe wall temperature. As shown, the difference in predictions using the two boundary conditions increases with increasing thermal conductivity in the pipe wall. This is due to the fact that increasing the thermal conductivity in the pipe wall causes a greater portion of the heat to be transferred longitudinally along the pipe walls and therefore leads to higher wall temperatures at the inlet to the pipe. This in turn implies higher heat transfer rates (higher  $\theta_b$ ) close to the inlet. From Fig. 3, it can be inferred that except in the vicinity of the pipe inlet, the solution is nearly insensitive to the choice of either boundary condition.

The increase in heat transfer due to finning is obvious in Fig. 4 (a 10-fold enhancement is seen for case 1), where the results of cases 1-3 are compared with the corresponding unfinned tube results (i.e., cases having the same thermal conductivity ratio as in cases 1-3 but with  $Bi_u = Bi_f = 1$ ). The heat transfer augmentation rates decrease with increasing thermal conductivity in the pipe wall because thermal conductivity smooths

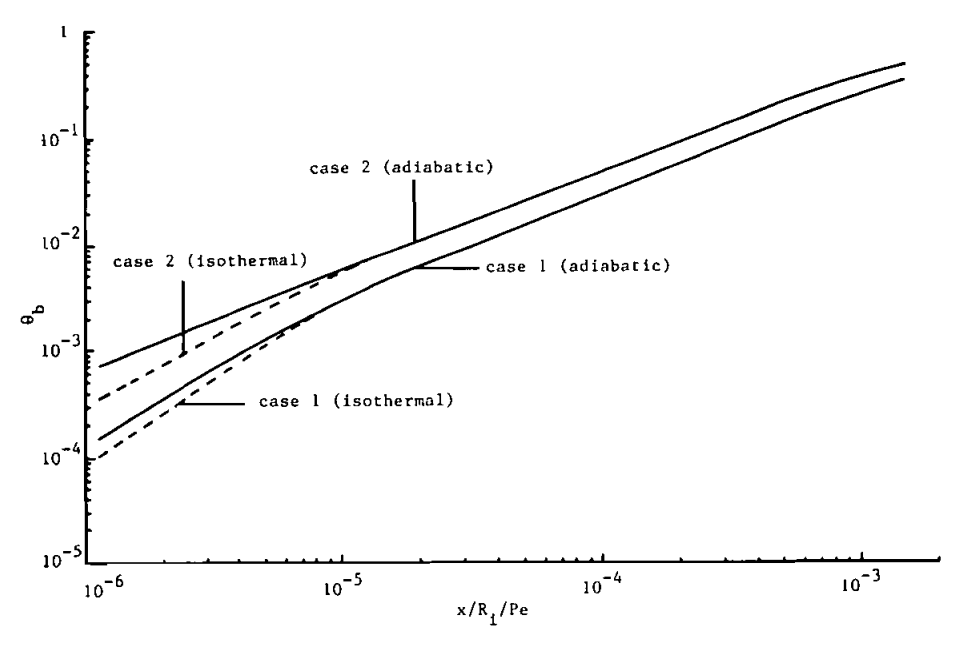


Fig. 3 The effects of adiabatic and isothermal boundary conditions on the streamwise bulk temperature, cases 1 and 2.

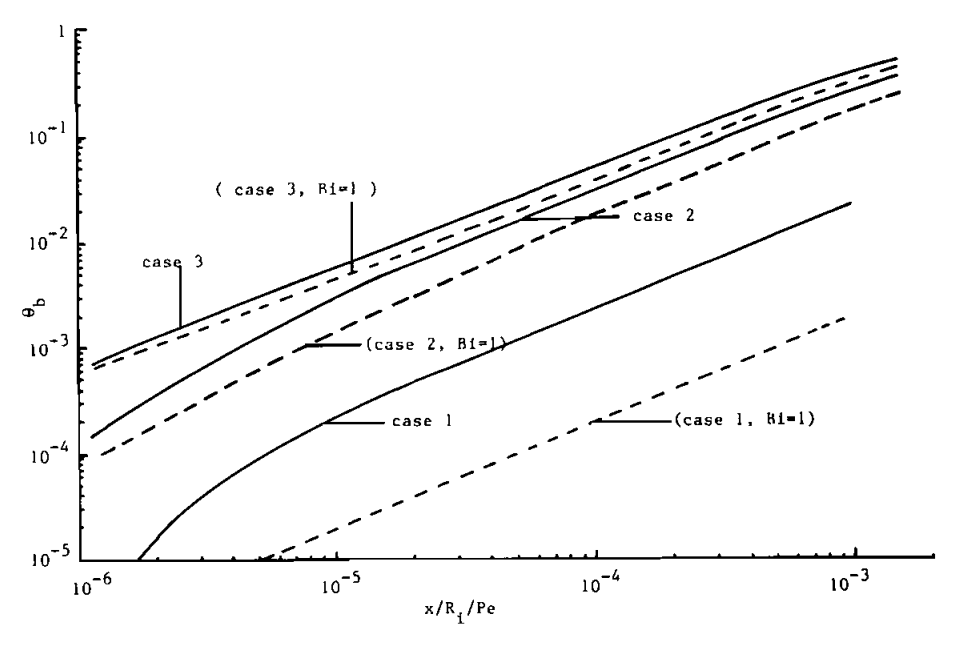


Fig. 4 The bulk temperature  $\theta_{\rm b}$  (or  $Q/Q_{\rm max}$ ) for axially periodic Biot number, cases 1-3, and the corresponding unfinned tube results (Bi = 1).

out the finning effect, especially at higher wall thermal conductivities. Furthermore, for all cases presented in Fig. 4, heat transfer enhancement diminishes with increasing streamwise distance along the pipe, where the fluid tends toward thermal saturation.

Figures 5-7 show the profiles for the fluid bulk temperature  $\theta_b$  (or  $Q/Q_{max}$ ) for both axially periodic Biot number cases and the corresponding uniform spatially averaged Biot number cases [Eq. (16)]. The streamwise periodic Biot number plots (cases 1, 2, and 3) are depicted by a solid line, whereas those for spatially averaged uniform Biot number (cases 1A, 2A, and 3A) are represented by dashed lines. In the absence of lengthy calculations for the periodic Biot number case, a constant Biot number solution may be considered as a first approximation for that case. The quality of this approximation is evaluated from the comparisons presented in Figs. 5-7.

In Fig. 5, it can be seen that there is substantial heat transfer enhancement when axial conduction along the pipe wall is considered (cases 2, 2A, 3, and 3A) as compared with situations when it is neglected (cases 1 and 1A). The largest values for  $\theta_b$  (or  $Q/Q_{max}$ ) occur for the highest wall conductivity (cases 3 and 3A). The increase in wall conductivity from 40 (case 2) to 400 (case 3) enhances heat transfer by a factor greater than 4 at the pipe inlet, and thereafter it tends to diminish somewhat with increasing downstream distance, where the fluid tends toward thermal saturation (i.e.,  $T_{bx} \rightarrow T_{\infty}$ ). This behavior can be explained by considering a control volume along the pipe wall. In the absence of axial wall conduction in the pipe, there is only transverse heat transfer through the control volume with  $q_o$  (heat transferred to the wall) equaling  $q_i$  (heat transferred to the fluid). In the presence of axial conduction, since  $T_{bx} \rightarrow T_{\infty}$  as  $X \rightarrow L_p$ , the axial wall conduction (assuming  $T_{\infty} > T_{in}$ ) is directed in the upstream direction (negative x direction), and hence at any X, due to this upstream conduction,  $T_{bx}$  (or  $Q/T_{bx}$ )

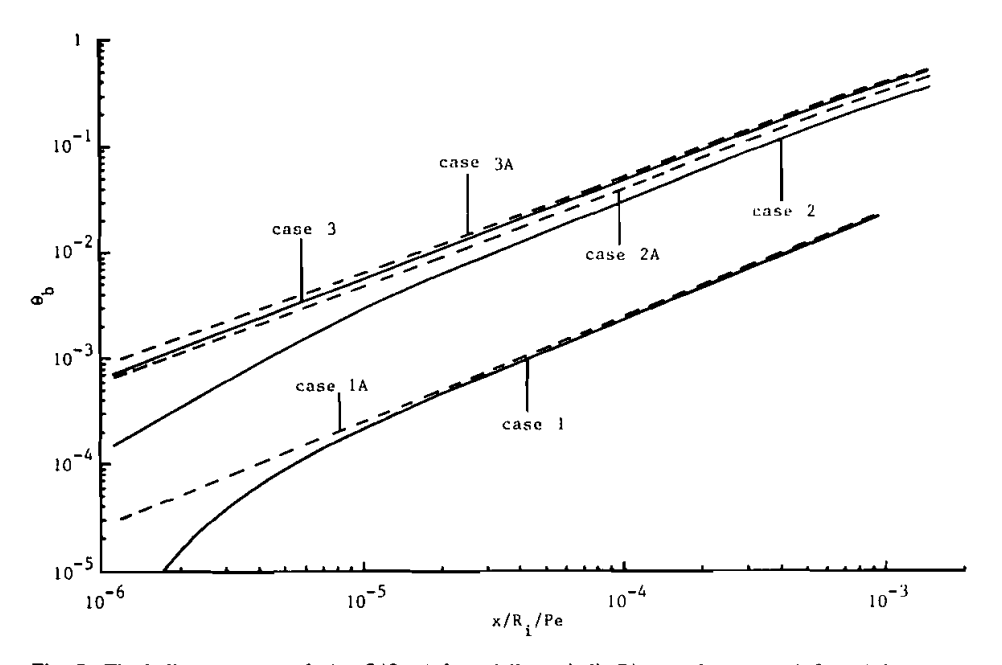


Fig. 5 The bulk temperature  $\theta_b$  (or  $Q/Q_{max}$ ) for axially periodic Biot number, cases 1-3, and the corresponding uniform Biot number, cases 1A-3A.

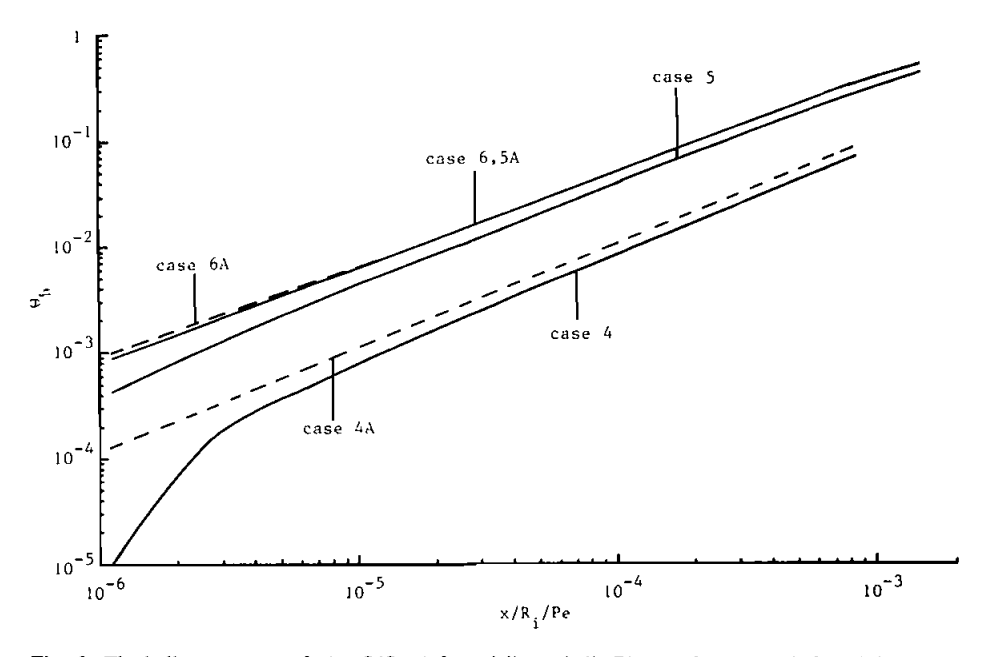


Fig. 6 The bulk temperature  $\theta_b$  (or  $Q/Q_{max}$ ) for axially periodic Biot number, cases 4-6, and the corresponding uniform Biot number, cases 4A-6A.

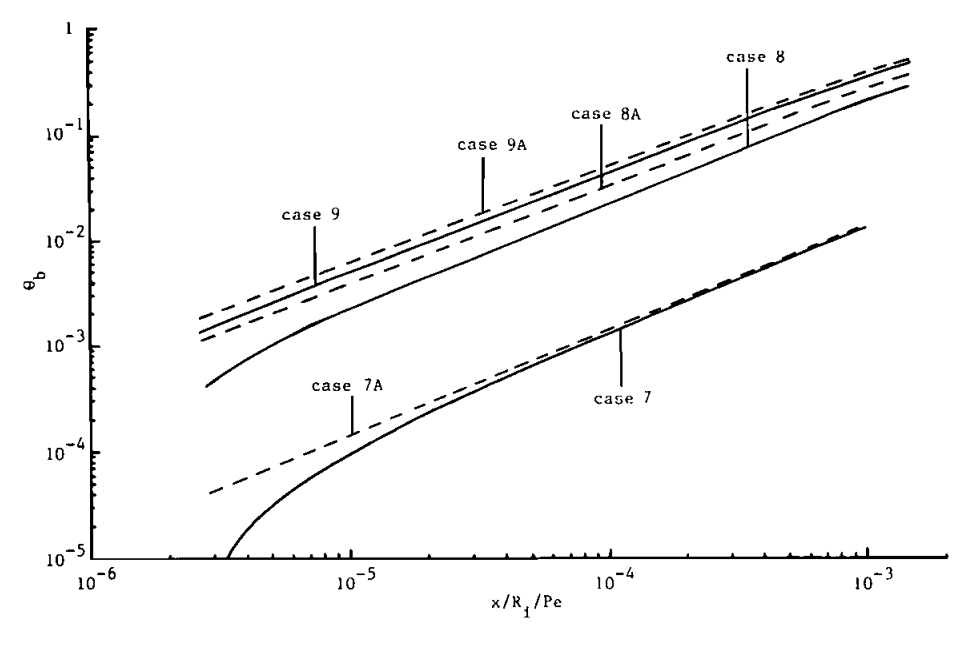


Fig. 7 The bulk temperature  $\theta_{\rm b}$  (or  $Q/Q_{\rm max}$ ) for axially periodic Biot number, cases 7-9, and the corresponding uniform Biot number, cases 7A-9A.

 $Q_{\text{max}}$ ) will be greater. Since axial conduction is stronger at higher values of the wall thermal conductivity,  $\theta_b$  is correspondingly higher.

In determining how well the results for the finned pipe can be approximated by the results for a uniform Biot number based on the spatial mean of  $Bi_u$  and  $Bi_f$ , it is clear that the approximating curves (cases 1A-3A) overestimate the heat transfer for the finned pipe. As seen in Fig. 5, the greatest overestimation occurs at X = 0 for all cases, and the approximating curves become increasingly more accurate at larger streamwise locations. Similar behavior is observed for cases 4A-9A presented in Figs. 6 and 7.

In Fig. 6, the Biot number is increased by a factor of 5 over the value used in Fig. 5. Increasing the pipe wall conductivity gives rise to a lower increase in heat transfer enhancement for cases 4-6 (Fig. 6) than for cases 1-3. Increasing the Biot number reduces the external convective thermal resistance and makes the internal convective thermal resistance more dominant. Hence, increasing the Biot number of the finned tube reduces the benefit from finning. In other words, with higher heat transfer coefficients, the pipe wall temperature is closer to  $T_{\infty}$  and is relatively more uniform (see Figs. 12 and 13), which reduces the effect of increasing the wall thermal conductivity. For the conducting cases, the spatially averaged Biot number results obtained are more accurate than those observed in Fig. 5.

Figure 7 reveals the geometrical effects on heat transfer behavior by presenting the results for cases 7-9. Here, the interfin spacing is 7 times the fin thickness, and the Biot numbers are the same as those for cases 1-3. By comparing Figs. 5 and 7, it can be seen that if the interfin spacing is increased, resulting in a decrease in the finned surface, the enhancement in heat transfer at the tube entrance due to increase in pipe wall conductivity is increased from a factor of 15 (in case 2) to a factor of 42 (for case 8). The unfinned surface, for case 8, is larger ( $\sigma = 7\tau$  as compared to  $3\tau$ ), and hence the fluid is less preheated along the finned segments. Thus the temperature difference ( $T_{\rm bx} - T_{\infty}$ ) is larger in the pipe entrance region and the fluid is more amenable to heat transfer. As a consequence, for this case, increasing the wall conductivity has a stronger effect. The accuracy of the constant Biot number approximating curves, cases 7A-9A, is somewhat less satisfactory than those depicted in Fig. 5.

#### **Nusselt Numbers**

The local Nusselt number is defined by

$$Nu = \frac{hD}{k_0} \qquad h = \left[ -k_0 \left( \frac{\partial T}{\partial r} \right)_{r-R_0} \right] / (T_w - T_{bx})$$
 (18)

The Nusselt number is averaged separately along each of the unfinned and finned segments of the pipe and is denoted by Nu, and Nu, respectively.

The streamwise variation of the Nusselt number for cases 1-3 is presented in Fig. 8, and for cases 4-6 in Fig. 9. The Nu values are plotted at the respective mid-points of the successive segments, and these points are connected with a smooth curve. All of the Nusselt number curves show similar behavior, decreasing with increasing downstream distance and then leveling off to a constant value, indicating the attainment of the thermally fully developed regime.

In Fig. 8, Nu<sub>f</sub> are higher than Nu<sub>u</sub>, as a result of the higher heat transfer rates

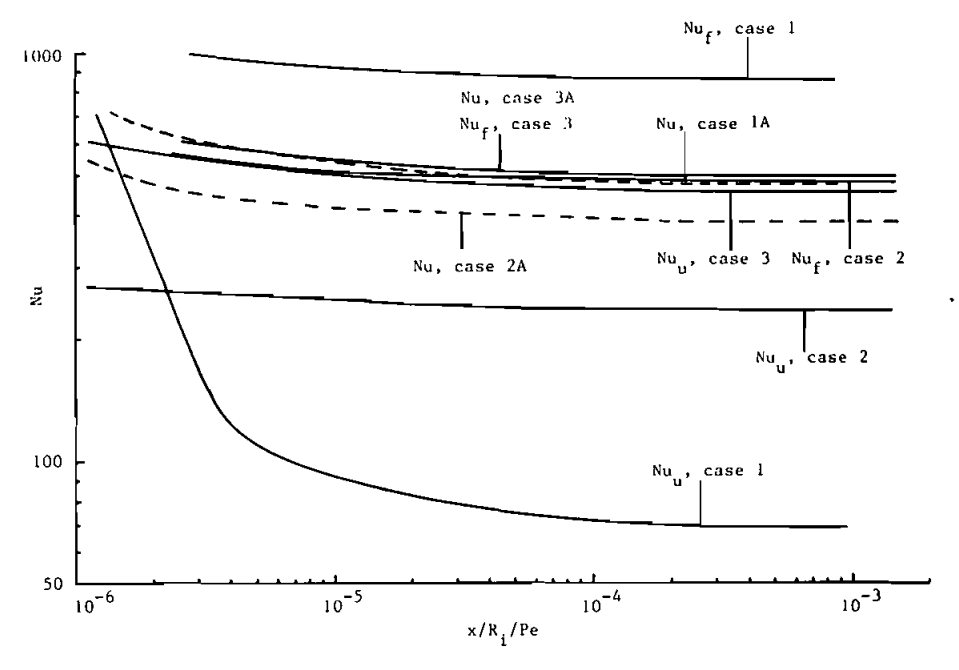


Fig. 8 Comparison between Nu variation for axially periodic Biot number, cases 1-3, and the corresponding uniform Biot number, cases 1A-3A.

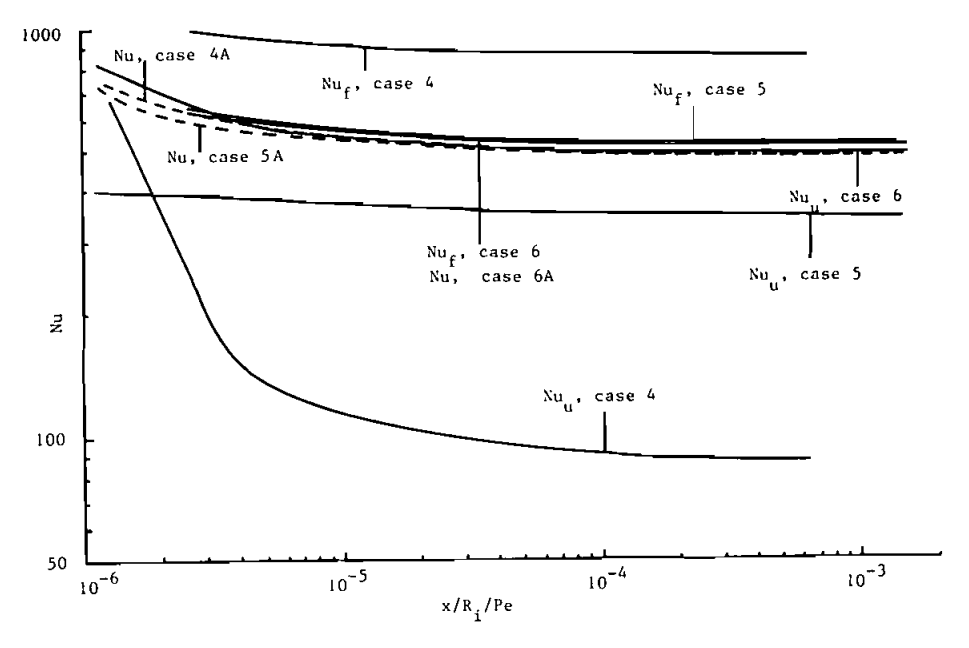


Fig. 9 Comparison between Nu variation for axially periodic Biot number, cases 4-6, and the corresponding uniform Biot number, cases 4A-6A.

occurring at the finned sections. The high rates are due to the higher Biot numbers along these sections, which in the physical situation represent the increased heat transfer area due to the fin. The value of the difference (Nu<sub>f</sub> - Nu<sub>n</sub>) decreases with increasing pipe wall conductivity, because axial conduction smooths the effect of finning. Thus when the pipe wall conductivity is high, the smoothing effect is stronger, and the differences in Nusselt number between the finned and unfinned sections decreases. For case 1 the Nu, values are well below and the Nu<sub>f</sub> values are higher than the corresponding values for cases 2 and 3. As noted above, this is due to axial conduction in cases 2 and 3, which tends to smear the abruptness of the changes between the Nusselt numbers in the unfinned and finned parts. The Nusselt numbers for the corresponding spatial average Biot number cases 1A-3A are also shown. The Nusselt numbers for these constant Biot numbers lie below the Nu<sub>f</sub> and above the Nu<sub>n</sub> numbers. For case 3, the Nusselt numbers for the periodic and the spatially averaged Biot number cases are so close that a single curve represents both. The highest error that occurs in assuming spatially averaged Biot numbers is for the case when the wall thermal conductivity is neglected (case 1). Thus, the constant Biot number [based on Eq. (16)] solution gives comparable Nusselt number results only when axial conduction is significant.

Figure 9 depicts the Nusselt number variation for cases 4-6. Here, the Biot number values are greater than those in Fig. 8 by a factor of 5. Inspection of Fig. 9 shows that the differences  $(Nu_f - Nu_u)$  are smaller here in comparison with those in Fig. 8. This is because in the presence of relatively high external heat transfer coefficients, the pipe wall temperature is closer to  $T_{\infty}$  (see Figs. 12 and 13). Therefore, the Nusselt number curves shown in Fig. 9 are closer to each other compared with the cases in Fig. 8. The other trends are similar to those given earlier (Fig. 8), and therefore the same discussion is not repeated. For the same reason, the Nusselt number variations for cases 7-9 are not presented.

Table 2 presents the axially averaged Nusselt numbers for the finned and unfinned sections of the pipe, defined by

$$\overline{\mathrm{Nu}}_{\mathrm{u}} = \sum_{i} \mathrm{Nu}_{\mathrm{u}}(x_{i}) \sigma \Big| \sum_{i} \sigma$$
 (19)

$$\overline{\mathrm{Nu}}_{\mathrm{f}} = \sum_{j} \mathrm{Nu}_{\mathrm{f}}(x_{j}) \tau / \sum_{j} \tau \tag{20}$$

Table 2 Axially Averaged and Periodically Developed Nusselt Number Value	Table 2	Axially	Averaged	and	Periodically	Developed	Nusselt	Number	Values
--	---------	---------	----------	-----	--------------	-----------	---------	--------	--------

Case	$\overline{Nu}_{\mathbf{u}}$	$\overline{Nu}_f$	$\overline{Nu}_{u,pd}$	$\overline{Nu}_{f,pd}$
1	103.21	930.11	69.12	858.88
2	248.45	512.62	233.73	482.44
3	490.36	532.53	455.14	499.25
4	118.14	915.18	87.39	849.21
5	372.07	556.39	340.77	517.12
6	522.53	548.43	485.72	507.37
7	73.21	995.87	58.84	902.15
8	223.42	474.28	206.92	443.76
9	428.56	526.17	417.61	507.32

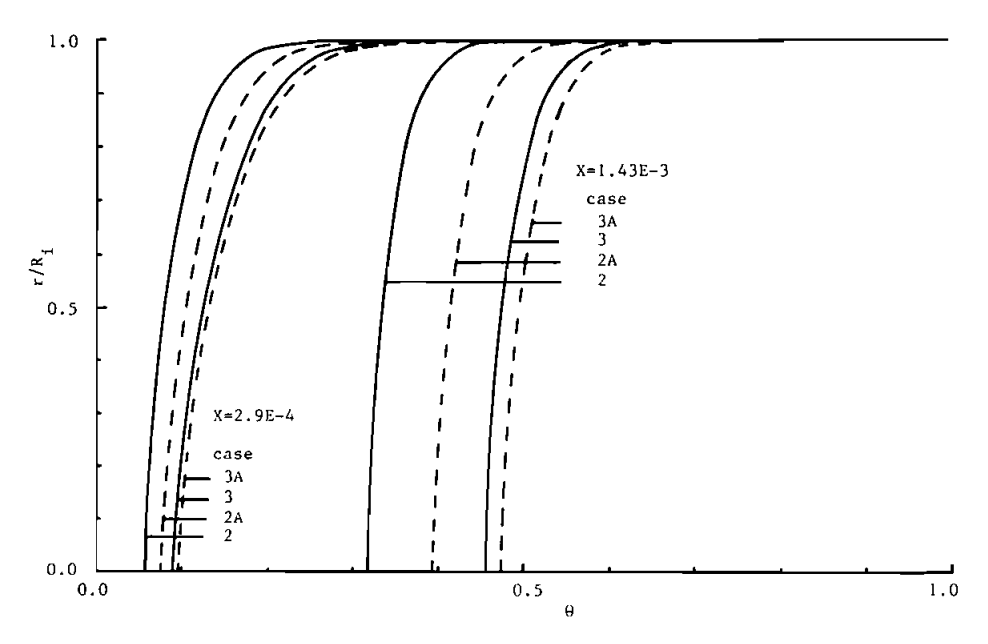


Fig. 10 Fluid temperature profile for axially periodic Biot number, cases 2 and 3, and the corresponding uniform Biot number, cases 2A and 3A.

The trends noted earlier also hold for these averaged values: the difference between the finned and unfinned Nusselt number values decreases with increasing wall conductivity and increasing magnitude of Biot number. The differences are more pronounced for increased interfin spacing.

Also presented in Table 2 are the corresponding asymptotic, periodically developed values. In long pipes, the use of the periodically developed values is expected to be reasonable, and the values in Table 2 confirm this expectation. For the conducting wall cases, the difference between the average and periodically developed values is less than 7% over the range of parameters considered. For the poorly conducting cases represented by cases 1, 4, and 7, the differences between the periodically developed and axially averaged values are significant. This observation is consistent with earlier comparisons of the Nusselt numbers with the constant spatially averaged Biot number solutions, where the agreement between the two solutions was satisfactory only for the high-conductivity cases.

#### **Temperature Distribution**

The fluid temperature profiles at two different cross-stream locations along the pipe, for some of the cases considered, are presented in Figs. 10 and 11. It is clear that all the temperature profiles in the pipe are characteristic for turbulent flow. Another common behavior of the temperature profiles is that the bulk temperature increases in the streamwise direction (compare temperature profiles at  $X = 1.43 \times 10^{-3}$  and  $X = 2.9 \times 10^{-4}$ ), which conforms with the bulk temperature variations depicted in Figs. 5-7. For all cases shown, the uniform, spatially averaged Biot number results overestimate the corresponding periodic Biot number predictions. This overestimation decreases in

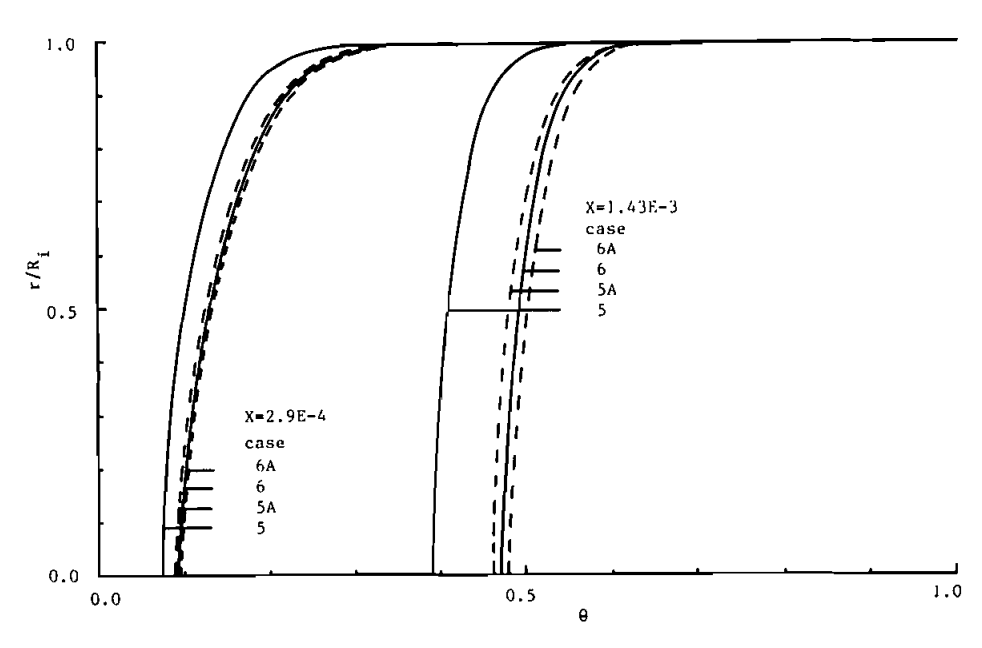


Fig. 11 Fluid temperature profile for axially periodic Biot number, cases 5 and 6, and the corresponding uniform Biot number, cases 5A and 6A.

the streamwise direction, where the fluid tends toward thermal saturation (Figs. 10 and 11). The overestimation also decreases with increasing values of thermal conductivity in the pipe wall (see the difference between cases 2 and 3 and cases 5 and 6) or higher levels of external heat transfer coefficient (see the difference between cases 2 and 5 and cases 3 and 6), where higher temperatures are involved.

In Figs. 12 and 13, temperature distributions in the pipe wall are presented for two intervals along the streamwise direction of the pipe. The high wall conductivity curves (cases 3, 6, and 9) exhibit a smooth monotonic variation due to the smoothing effect of axial conduction in the pipe wall. The maximum smoothing is obtained with the largest external heat transfer coefficients because the pipe wall temperature is then closer to  $T_{\infty}$ . With decreasing wall conductivity values, the smoothing effect of axial conduction is reduced, and the temperature curves (cases 2, 5, and 8) show a highly nonmonotonic periodic variation with high values in the finned regions and low values in the unfinned regions. The amplitude of these variations [i.e., the difference between the highest and lowest temperature values over the segment  $n(\sigma + \tau) < X < (n + 1)(\sigma + \tau)$ ] increases with decreasing external heat transfer coefficient or increasing interfin spacing. This is due to the fact that increasing the external heat transfer coefficient or decreasing the interfin spacing tends to increase the temperature in the unfinned parts of the pipe without appreciably affecting the maximum temperature in the finned sections.

Finally, the present turbulent results are qualitatively compared with those for laminar flow reported by Sparrow and Charmchi [1] and Moukalled and Acharya [2]. Obviously, a direct comparison is not attempted, since the Reynolds numbers are different. Due to the higher internal heat transfer coefficient in turbulent flow, which results in higher cooling rates, the pipe wall temperature is lower than the temperature asso-

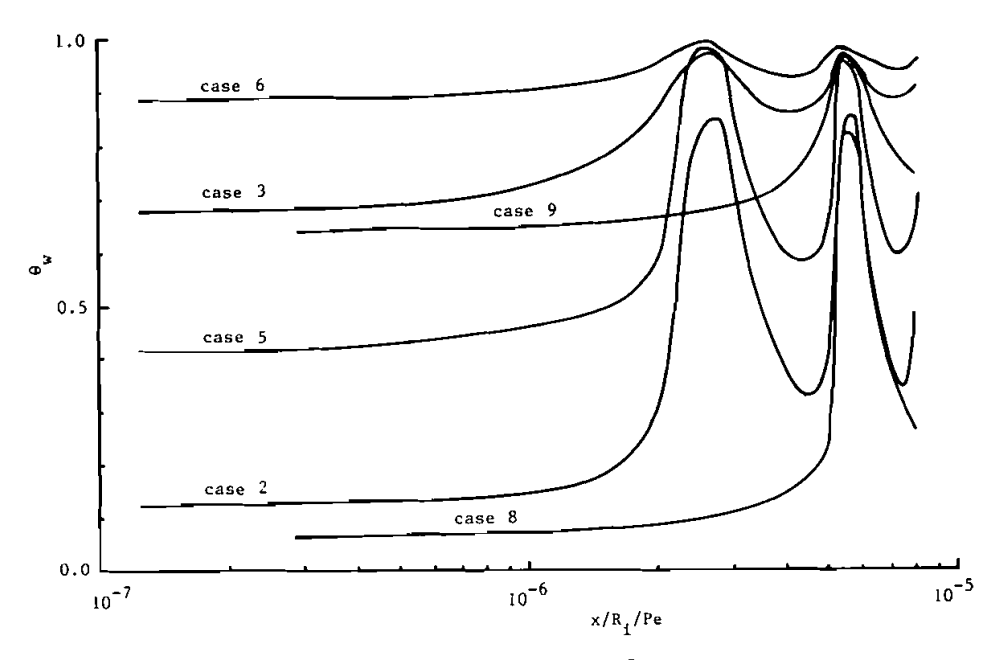


Fig. 12 Pipe wall temperature distributions for  $10^{-7} < x/(R_i \text{ Pe}) < 10^{-5}$ .

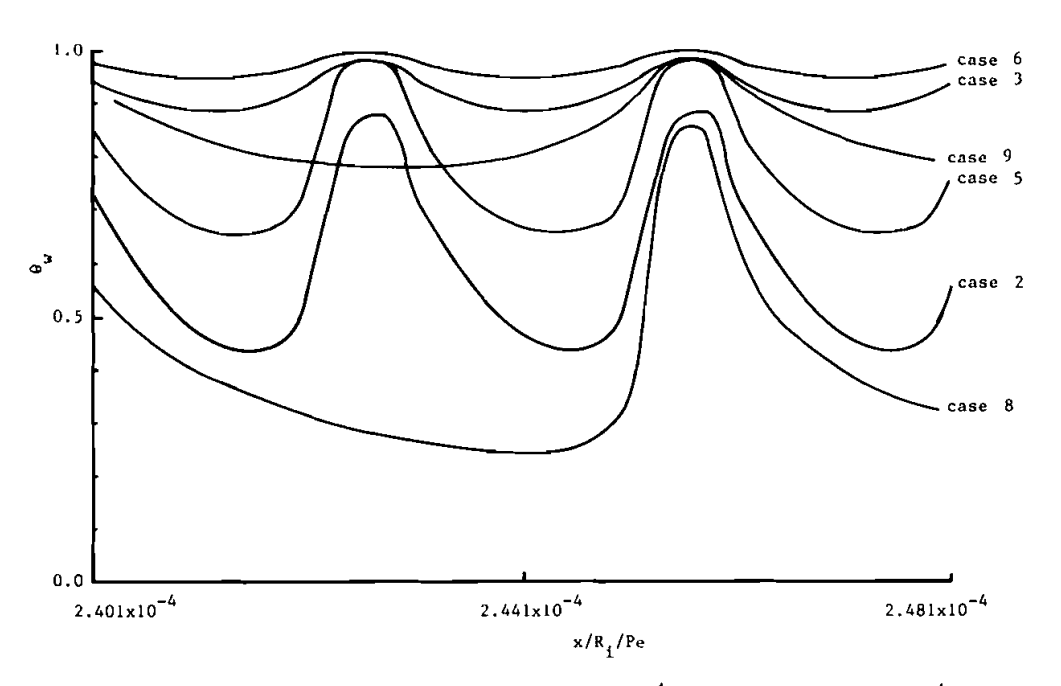


Fig. 13 Pipe wall temperature distributions for  $2.401 \times 10^{-4} < x/(R_i \text{ Pe}) < 2.481 \times 10^{-4}$ .

ciated with laminar flow. Also, that axial conduction in the pipe wall is relatively more important in turbulent flow is reflected by the larger underestimation of the heat transfer rates when conductivity effects are not accounted for.

#### **CLOSING REMARKS**

The influence of axial wall conduction on turbulent convection heat transfer in an externally finned circular tube is studied numerically. Results indicate a strong dependence of heat transfer on axial conduction in the tube walls. Increasing the wall thermal conductivity reduces the benefit of finning, while increasing the interfin spacing enhances the role of the wall thermal conductivity. Also, at constant wall conductivity, increasing the interfin spacing causes a decrease in heat transfer rates. The effects of wall conduction decrease as the level of the external convection heat transfer coefficient is increased. Moreover, the difference between finned and unfinned Nusselt number values decreases with increasing wall thermal conductivity. When the tube wall conductivity is large, the wall temperatures indicate a smooth variation along the length of the tube, but exhibit a periodically decaying profile when the tube wall conductivity is low. A constant spatially averaged Biot number solution is found to give comparable heat transfer results only for the higher wall conductivity cases. The asymptotically developed finned and unfinned Nusselt numbers compare with the axially averaged values for the conducting wall cases to within 7%.

#### **REFERENCES**

- E. M. Sparrow and M. Charmchi, Laminar Heat Transfer in an Externally Finned Circular Tube, ASME J. Heat Transfer, vol. 102, pp. 605-611, 1980.
- F. Moukalled and S. Acharya, Forced Convection Heat Transfer in a Finitely Conducting Externally Finned Pipe, ASME J. Heat Transfer, vol. 110, pp. 571-576, 1988.
- Y. K. Lin and L. C. Chow, Effects of Wall Conduction on Heat Transfer for Turbulent Flow in a Circular Tube, ASME J. Heat Transfer, vol. 106, pp. 597-604, 1984.
- M. Faghri and E. M. Sparrow, Simultaneous Wall and Fluid Axial Conduction in Laminar Pipe-Flow Heat Transfer, ASME J. Heat Transfer, vol. 102, pp. 58-63, 1980.
- N. K. Anand and D. R. Tree, Some Studies of the Effects of Axial Conduction in a Tube Wall on the Steady State Laminar Convective Heat Transfer, ASME J. Heat Transfer, vol. 109, pp. 1025-1028, 1987.
- R. M. Fithen and N. K. Anand, Finite Element Analysis of Conjugate Heat Transfer in Axisymetric Pipe Flows, Numer. Heat Transfer, vol. 13, pp. 189-203, 1988.
- G. S. Barozzi and G. Pagliarini, A Method to Solve Conjugate Heat Transfer Problems: The Case of Fully Developed Laminar Flow in a Pipe, ASME J. Heat Transfer, vol. 107, pp. 77– 83, 1985.
- 8. H. M. Soliman, Analysis of Low Péclet Heat Transfer during Slug Flow in Tubes with Axial Wall Conduction, ASME J. Heat Transfer, vol. 106, pp. 782-788, 1984.
- E. K. Zariffeh, H. M. Soliman, and A. C. Trupp, The Combined Effects of Wall and Fluid Axial Conduction on Laminar Heat Transfer in Circular Tubes, *Proc. 7th Int. Heat Transfer Conf.*, vol. 3, pp. 131-135, 1985.
- H. Schlichting, Boundary Layer Theory, 7th ed., pp. 475-531, McGraw-Hill, New York, 1960.
- 11. L. Prandtl, Uber die Ausgebildete Turbulenz, Zamm, vol. 5, p. 136, 1925, and Proc. 2nd Int. Cong. Appl. Mech., Zurich, 1926.

- 12. J. Nikuradse, Gesetzmassigkeit der turbulenten Stromung in glatten Rohren, *Forschungshet*, 356, 1932.
- 13. E. R. Van Driest, On Turbulent Flow near a Wall, J. Aero. Sci., vol. 23, pp. 1007-1011, 1956.
- 14. S. V. Patankar and D. B. Spalding, *Heat and Mass Transfer in Boundary Layers*, Intertext Books, London, 1970.
- 15. S. V. Patankar, Numerical Heat Transfer and Fluid Flow, Hemisphere, Washington, D.C., 1980

Received 14 December 1990 Accepted 18 June 1991